ELSEVIER

Nuclear Instruments and Methods in Physics Research A 471 (2001) 374–379

NUCLEAR INSTRUMENTS & METHODS IN PHYSICS RESEARCH Section A

www.elsevier.com/locate/nima

Pulse shape discrimination of charged particles with a silicon strip detector

J. Lu[a], P. Figuera[a,*], F. Amorini[a], G. Cardella[b], A. DiPietro[a], A. Musumarra[a], M. Papa[b], G. Pappalardo[a,c], F. Rizzo[a,c], S. Tudisco[a,d]

[a] *INFN-Laboratori Nazionali del Sud, Via S.Sofia 44, I-95123 Catania, Italy*
[b] *INFN-Sezione di Catania, Corso Italia 57, I-95129 Catania, Italy*
[c] *Dipartimento di Fisica ed Astronomia, Universita' di Catania, Corso Italia 57, I-95129 Catania, Italy*
[d] *Centro Siciliano di Fisica Nucleare e di Struttura della Materia, Corso Italia 57, I-95129 Catania, Italy*

Received 20 July 2000; received in revised form 13 October 2000; accepted 24 November 2000

Abstract

A simple and effective pulse shape discrimination technique is applied to a silicon strip detector array. Excellent charge identification from H up to the Ni projectile has been obtained and isotope separation up to N has also been observed. The method we systematically studied is essentially based on a suitable setting of the constant fraction discriminators, and its main advantage is that no additional electronic modules are needed compared to the ones used in the standard TOF technique.

PACS: 29.40.Wk

Keywords: Pulse shape discrimination; Silicon detectors; Constant fraction discriminator

1. Introduction

Since the early sixties, it has been known that the shape of signals from solid state detectors can be used for particle identification (e.g. [1]). Recently, this idea has been deeply revised in a group of papers by Pausch et al. [2–6], where it has been shown that the shape of current signals from solid state detectors is mainly governed by the combination of plasma erosion time and charge carrier collection time effects. When ions are injected from the rear side (i.e. opposite to the junction side) the two effects act coherently, and pulse shape differences for different incident ions are enhanced [3]. Different methods have been proposed in [2–6] to extract information on the incident ions from the pulse shape showing that, for rear side injection, a good identification can be obtained with energy thresholds down to ~ 3.0 and ~ 4.0 MeV/nucleon for Z ranging between 6 and 11, respectively (e.g. [5,6]). Even though some of the proposed methods are rather simple, they all require the use of a dedicated electronic chain. Therefore their application to existing or new silicon multi-detectors would introduce non negligible costs.

*Corresponding author. Fax: +39-095-7141815.
E-mail addresses: lu@lns.infn.it (J. Lu), figuera@lns.infn.it (P. Figuera).

0168-9002/01/$ - see front matter
PII: S0168-9002(01)00805-1

In the present paper we will present the results of a systematic study on a pulse shape identification method based on the use of the same electronic chain normally used in the conventional time of flight technique. The clear advantage of this method is that it can be easily applied also to existing multi-detectors with no need of a new dedicated electronic chain. The method is based on the use of charge preamplifiers, low polarization voltages, rear side injection of the incident particles and on a proper setting of the constant fraction discriminators which enhances the dependence of the timing output on the rise time of the input signals. Parallel to us Prete et al. [7] applied a method based on the same ideas to a Si multidetector, showing satisfactory identification up to charge $Z = 6$.

2. Experimental details

The on beam tests have been performed at the cyclotron of the Laboratori Nazionali del Sud in Catania, using a 25.7 MeV/nucleon ^{58}Ni beam impinging on a 3 mg/cm^2 ^{51}V and ^{45}Sc composite target. The studied PSD method has been applied to the first stage of the Si–CsI(Tl) hodoscope of the Trasma multidetector [8]. The first stage of the hodoscope is a 300 μm thick, ion implanted, silicon annular strip detector with an inner radius of about 16 mm and an outer radius of about 88 mm. The detector, manufactured by Eurisys Mesures (Type IPS13 · 73 · 74-300-N9), consists of 8 independent sectors each divided into 9 circular strips and was placed 80 cm downstream the target location. A sketch of a single sector is shown in Fig. 1 and specifications are reported in Table 1. The block scheme of the electronics for a single strip is shown in Fig. 2. The signals from each strip are first processed by a charge preamplifier (eV-5092) so that the original pulse shape differences are mainly reflected by different rise times of the output signals. The preamplifier is followed by a shaping amplifier and a timing amplifier (Silena-761F/R—16 channel shaping + timing amplifier). The energy signal is then integrated and converted by a QDC (Caen-VN1465S 64 channels VME QDC). The use of these highly integrated and

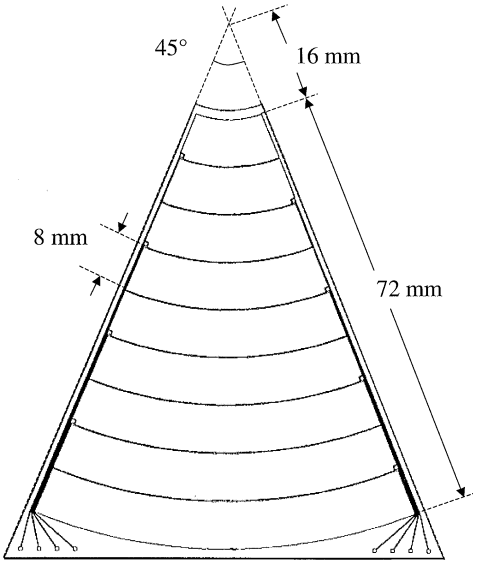

Fig. 1. Sketch of a single sector of the used detector consisting of 9 circular strips on the same silicon slice. Eight of such sectors form a complete circular detector having a central hole of about 30 mm and an external radius for the last strip of about 88 mm.

Table 1
Factory specifications of the detector type used in our tests

Type	Resistivity (kΩ cm)	Depletion voltage (V)	Recommended operating voltage (V)
Eurisys IPS 13 · 73 · 74-300-N9	10	35	40

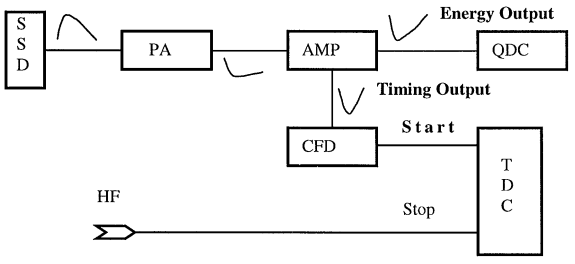

Fig. 2. Block scheme of the electronics for a single strip. SSD-silicon strip detector; PA-charge preamplifier; AMP-spectroscopy amplifier + timing amplifier; CFD-constant fraction discriminator; QDC-charge to digital converter; TDC-time to digital converter; HF-Cyclotron radio frequency time reference. See text for details.

double dynamics QDCs allows to easily handle large energy ranges and improves noise rejection. However we verified that good charge identification can be obtained also using a more "conventional" ADC. The timing signal, whose rise time reflects the original pulse shape information, is sent to a constant fraction discriminator (CDF) (Caen-C208 16 channels CAMAC-CFD). Our goal is now to enhance the dependence of the CFD timing output on the charge, mass and energy of the ions impinging on the detector. To enhance the Si detector pulse shape differences for different ions and energies, we did not overbias the detector using (with rear side injection) the factory suggested operating voltage of 40 V, only slightly above the full depletion one (see Table 1). In addition we operated the CFDs with rather large delays and fraction settings to maximize the dependence of the CFD output time on the rise time of the input signals. In the next section we will systematically investigate how the "quality" of particle identification depends on the CFD settings. Using the Cyclotron HF as reference, the measured "time", carrying information on the original pulse shape (t_{PS} in the following), is converted by a TDC (Caen-VN1488S 64 channels VME TDC). The cyclotron has been operated in a pulse suppression mode corresponding to a time dynamics between two beam bursts of 155 ns and intrinsic burst width of about 1.5 ns.

Note that low cost and highly integrated electronics was used for this tests. In addition we also verified that results similar to the ones we will discuss in the next section can be obtained using preamplifiers, amplifiers, CDFs and converters of other kinds.

3. Results and discussion

In this section we will present the obtained results, and discuss how the identification "quality" depends on the fraction and delay settings of the CFDs.

As an example, in Fig. 3a we show a scatter plot of t_{PS} versus energy (low gain QDC output) obtained with a fraction setting $F = 0.33$ and a delay setting of 100 ns. Fig. 3b represents the same spectrum as Fig. 3a but the energy corresponds to the high gain output of the QDC. A clear charge identification from H up to the Ni projectile is observed in a wide energy range extending up to

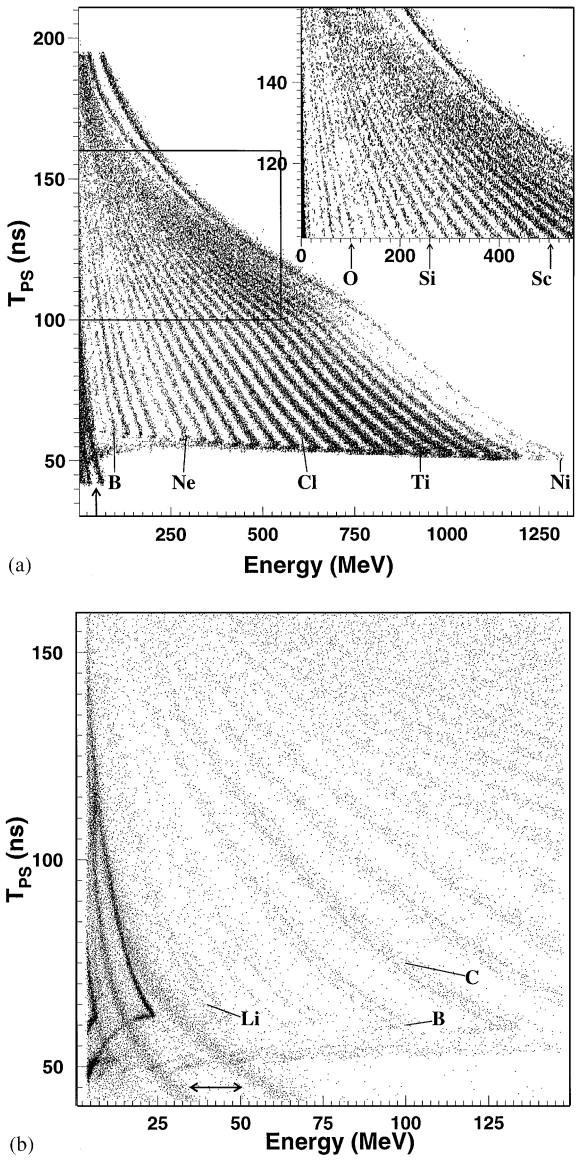

Fig. 3. (a) The E–t_{PS} scatter plot obtained with a CFD fraction setting $F = 0.33$ and a CFD delay time of 100 ns. The region marked by a box is expanded in the inset. (b) Same E–t_{PS} plot as Fig. 3a, but for the high gain conversion output of the QDC. In both figures the events in the branches marked by the arrows are due to low energy heavy particles whose t_{PS} range is larger then the interburst time. The time scale is calibrated in ns with an arbitrary choice of the $t_{PS} = 0$ instant.

the punch through energies for the different ions. Typical charge identification thresholds are ~ 1.7 MeV/nucleon for $Z \approx 6$, ~ 3.0 MeV/nucleon for $Z \approx 11$ (Fig. 3b) and ~ 5.5 MeV/nucleon for $Z \approx 20$ (inset in Fig. 3a). Isotope identification up to $A \approx 13$ is observed with an energy threshold of about 6 MeV/nucleon (Fig. 3b). Unfortunately, the experimental t_{PS} range for heavier particles is larger than the beam interburst time used in the present test. Therefore branches corresponding to low energy heavy particles (marked by arrows in Fig. 3) "wrap round" and are observed at low t_{PS} times blurring the identification for low energy particles. Note that the measured t_{PS} is a combination of pulse shape effects and real time of flight. However, the real time of flight difference, between two adjacent charges at a fixed incident energy, typically accounts only for 20% or less of the time difference measured and is of the same order as our time resolution. Therefore the observed particle identification is essentially due to pulse shape effects. It is interesting to note that in the present case the threshold for charge identification is due to the merging of different charge branches at low energy, while in previous papers by Pausch et al. (e.g. [4–6]) and also in the very recent paper of Mutterer et al. [9] the identification threshold is due to the bending back of different charge branches at low energy. Even if at very low energy the real TOF contribution is no more negligible in our case (e.g. about 40% of the measured t_{PS} difference between C and B around 20 MeV), the TOF contribution alone is not sufficient to explain the two different behaviors whose origin is at present not well understood.

We have now to discuss how the identification "quality" depends on the fraction and delay settings of the CFDs. To quantitatively evaluate this "identification quality" we use the energy threshold for particle identification and the "resolving power" M for the charge separation which we defined in the following way:

$$M = 0.5 \frac{\Delta T}{\Delta Z \, \Delta \delta}.$$

Here ΔT, ΔZ, and $\Delta \delta$ have the following meaning. In the E–t_{PS} plot, we divided the energy range into fixed width bins. We then projected each energy bin onto the time axis observing peaks corresponding to the different charges. ΔT is the t_{PS} interval between two peaks, ΔZ is the corresponding charge difference and $\Delta \delta$ is the average standard deviation σ of these two peaks extracted with gaussian fits. The so defined M factor may remind a similar factor [10] frequently used to characterize the n–γ discrimination ability. In Fig. 4 we show a projection onto the t_{PS} axis of the spectrum in Fig. 3a, corresponding to an energy bin $E = 300 \pm 5$ MeV, which has been used to extract the corresponding M-factor ≈ 2.6 (square symbol) of Fig. 6. The continue line represents a fit with six gaussians which has been used to extract σ for the Na and S peaks. In order to compare identification energy thresholds obtained with different CFD settings, we defined the following standard procedure to estimate the thresholds and their associated uncertainty. In the E–t_{PS} 2D spectrum we performed a fit of the different charge branches, in a low energy region where different charges were still clearly separated. These fits were then extrapolated to lower energy. The intersection point of two neighboring fit lines, taking into

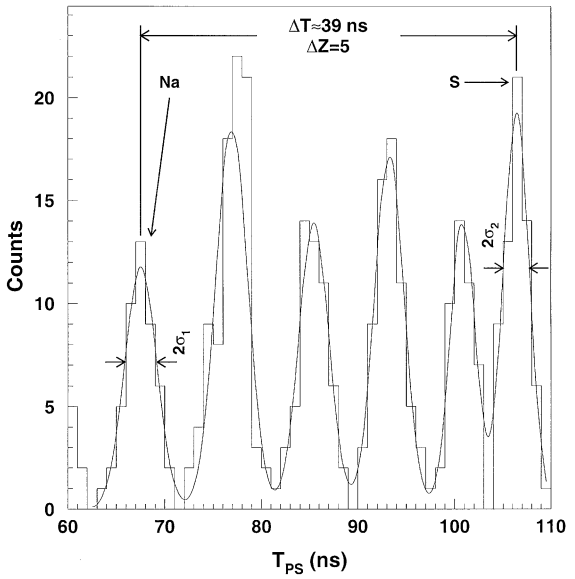

Fig. 4. Projection onto the t_{PS} axis of the spectrum in Fig. 3a (histogram), corresponding to an energy bin $E = 300 \pm 5$ MeV and a t_{PS} range 60–110 ns. The full line represents a fit with six gaussians. The TOF contribution on the measured t_{PS} difference between adjacent ions is of the order of 10% in the present case.

Table 2
Energy thresholds and charge separation "resolving power" M, obtained with different CFD delays for a fixed fraction setting $F = 0.6$. The M factor values were extracted at energies of 300 and 600 MeV (see text for details)

Delay time (ns)	Energy threshold (MeV)			M Factor	
	B	C	N	300 MeV	600 MeV
60	20 ± 2	23 ± 2	26 ± 2	2.56	2.68
100	16 ± 1	20 ± 1	24 ± 1	3.07	2.99

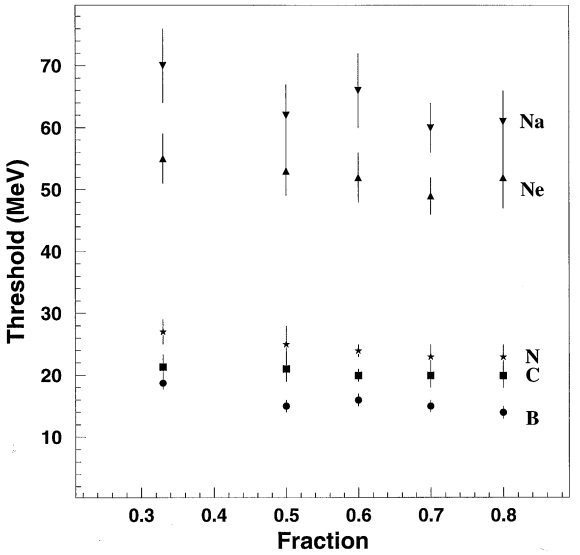

Fig. 5. Observed threshold variation as a function of the CDF fraction setting for a fixed CFD delay of 100 ns.

account their finite widths due to the experimental resolution, defined the energy threshold. After defining the parameters which quantitatively reflects the identification "quality" (identification energy threshold and M factor) we can discuss their observed dependence on the CFD setting.

It is well known that operating the CFD with small delay times (ARC mode) one can at least partially compensate for different input rise times. Since our goal is now the opposite, one qualitatively expects to obtain a better identification for larger CDF delay settings. This is exactly what has been observed. As an example, in Table 2 we report some energy thresholds and M factor values

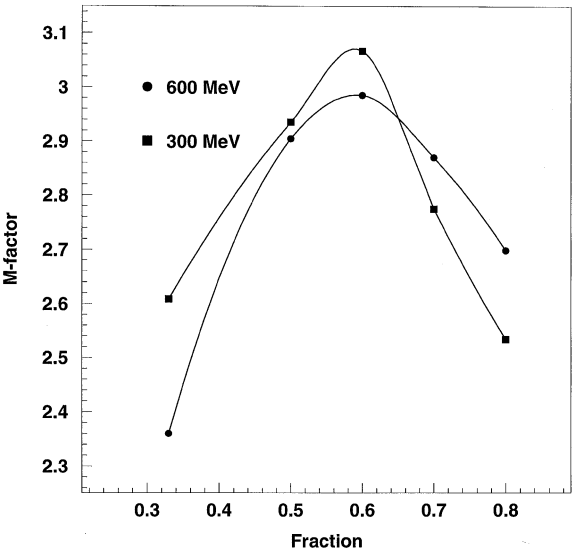

Fig. 6. Observed M factors as a function of the CDF fraction setting at $E = 600$ MeV (full circles) and $E = 300$ MeV (full squares) for a fixed CFD delay of 100 ns. See text for details.

corresponding to two different delay times for a fixed CFD fraction setting $F = 0.6$. As one can see, both the thresholds and the M factors improve by increasing the delay, therefore we decided to keep it constant at 100 ns (i.e. the maximum possible delay setting in our modules).

In Fig. 5 the identification thresholds for different elements are reported as a function of the fraction setting, for a constant delay of 100 ns. As one can see the pulse shape discrimination threshold is a weak function of fraction setting, slightly decreasing for increasing fractions. Finally, in Fig. 6, we show the observed dependence of the M factor as a function of the fraction setting, again for a constant delay of 100 ns. The M factors have been extracted using the same procedure as in Table 2 by considering the peaks of Ca and Cr at $E = 600$ MeV and the peaks of Na and S at $E = 300$ MeV with an energy bin of ± 5 MeV. As one can see relatively large fractions, of the order of 0.5–0.6, give the best results for particle identification. This result was qualitatively expected. In fact, as a preliminary test, we digitized some output signals from the timing amplifier, and observed the simulated CFD zero crossing

calculated for these signals with a simple program. Larger zero crossing time ranges were observed for larger fraction settings, in qualitative agreement with the above presented experimental results.

The method discussed in the present paper has been applied to all the strips of the 8 independent sectors of our detector, and already successfully used in a real experiment [11]. Similar identification scatter plots were obtained with different complete detectors of the same type.

4. Conclusions

In summary, a good identification from H up to the Ni projectile has been observed with energy thresholds comparable or better (especially for low charges around $Z \approx 6$) than the ones obtained in [2–6]. The most prominent features of the method we studied are that no additional electronic modules are needed compared to the conventional TOF technique, and that commercial and highly integrated electronics can be used. Therefore the method appears to be very promising, especially for its possible application to existing silicon multidetectors with no additional costs for new dedicated electronic chains.

References

[1] C.A.J. Ammerlaan et al., Nucl. Instrum. and Meth. 22 (1963) 189.
[2] G. Pausch et al., Nucl. Instrum. and Meth A 322 (1992) 43.
[3] G. Pausch et al., Nucl. Instrum. and Meth A 337 (1994) 573.
[4] G. Pausch et al., Nucl. Instrum. and Meth A 349 (1994) 281.
[5] G. Pausch et al., Nucl. Instrum. and Meth A 365 (1995) 176.
[6] G. Pausch et al., IEEE Trans. Nucl. Sci. 43 (1996) 1097.
[7] G. Prete et al., Nucl. Instrum. and Meth. A 422 (1999) 263.
[8] A. Musumarra et al., Nucl. Instrum. and Meth. A 370 (1996) 558.
[9] M. Mutterer et al., IEEE Trans. Nucl. Sci. 47 (2000) 256.
[10] G.F. Knoll, Radiation Detection and Measurements, 2nd Edition, Wiley, New York, 1989, p. 646.
[11] S. Tudisco et al., Proceedings of Experimental Nuclear Physics in Europe, Sevilla, Spain, AIP Conference proceedings, Vol. 495, June 1999, p. 323.